NJC

PAPER

View Article Online
View Journal

Cite this: DOI: 10.1039/c5nj00364d

Development of halogen-free flame retardant phosphazene and rice husk ash incorporated benzoxazine blended epoxy composites for microelectronic applications

Krishnamoorthy Krishnadevi and Vaithilingam Selvaraj*

Received (in Montpellier, France)
10th February 2015,
Accepted 17th June 2015

DOI: 10.1039/c5nj00364d

www.rsc.org/njc

The present study is focused on the synthesis and characterization of flame retardant amine-terminated cyclophosphazene and silane functionalized rice husk ash reinforced benzoxazine blended epoxy composites as a halogen-free flame retardant material (ATCP/FRHA/Bz-Ep). FT-IR spectroscopy, scanning electron microscopy (SEM), X-ray diffraction analysis, contact angle measurements, dielectric constant, DSC, TGA, UL-94, LOI and cone calorimetry were used to characterize the surface morphology as well as the structural, electrical, thermal and flame retardant properties of the resultant ATCP/FRHA/Bz-Ep composite material. The experimental results suggested that ATCP/FRHA/Bz-Ep composites exhibit better flame retardant and dielectric performance compared to that of a neat Bz–Ep material. A plausible mechanism of the fire retardant ATCP/FRHA/Bz-Ep composite material is hypothesized based on the results of cone calorimetric, thermal and electrical analysis. From the abovementioned results, it was concluded that the ATCP/FRHA/Bz-Ep composite can be used as an electrical resistant material for electronic and microelectronic applications.

Introduction

Polymer composites can be used in various high performance applications due to their light-weight, which is as an essential and desirable property required for sustainable flame retardant polymers. Flame retardants are one of the most important additives for combustible polymers to improve their fire resistant properties.[1–3] Flame retardant materials are used to reduce combustibility and toxic fume production of the polymers, which are pivotal requirements for the development and application of new materials.

Epoxy resins are high performance thermosetting resins possessing many attractive properties such as high mechanical strength, good adhesion,[4] good electrical insulation properties,[5] low cost and ease of formation.[6] However, epoxy resins are easily flammable and they are unable to satisfy some high performance flame retardant applications. In general, the flame retardant property of epoxy resins can be improved by adding flame retardant additives or by incorporating reactive flame retardants.

The most effective flame retardants are halogen containing chemicals, but they usually release harmful toxic gases as well as heavy smoke during the combustion process. Though the halogen containing flame retardants attract great attention, they still face significant challenges in both academic and industrial applications. However, brominated flame retardants in particular are restricted in many countries due to the migration of toxic by-products such us hydrogen bromide and dioxins[7] to the environment during combustion process.

The abovementioned drawbacks tempt researchers to develop innovative and eco-friendly halogen-free polymeric materials for electronic, electrical, aerospace and transportation applications. Amongst all the halogen-free flame retardants, scientists are introducing nitrogen-, phosphorous- and silica-based intumescent flame retardants as additives for achieving flame retardant performance.

Due to prominent processability, the excellent thermal and mechanical properties of epoxy-modified benzoxazine blended systems have attracted increasing attention in a wide range of applications, including adhesives, filler-reinforced composite materials, and coatings for electronic circuits.[8–11] However, the absence of inorganic materials in the benzoxazine blended epoxy systems means they have low flame retardant capacities that are inadequate for the fire resistance properties of the materials. Therefore, effective and eco-friendly inorganic flame retardant materials should be incorporated in the Bz–Ep composites in order to enhance their flame resistance properties. Rice husk ash is a biomass waste material, and it contains a

Nanotech Research Lab, Department of Chemistry, University College of Engineering, Villupuram (A Constituent College of Anna University, Chennai), Kakuppam, Villupuram-605 103, Tamil Nadu, India. E-mail: rajselva_77@yahoo.co.in, vselva@aucev.edu.in; Fax: +91-4146-224500

rich source of silica. In general, the utilization of biomass rice husk ash in the composites has brought several advantages such as low density, greater deformability, less abrasiveness to equipment, biodegradability and low cost. Hence, the present study attempts to obtain low k values, improved thermal and high performance flame retardant properties and improved hydrophobicity using eco-friendly bio-waste materials like rice husk ash.

Phosphazenes are a well-known class of versatile functional materials with an inorganic backbone structure. When phosphazenes are appropriately substituted, the resultant materials can be employed as flame resistant materials, elastomers, membranes, solid ionic conductors and inert biomaterials.[12] Such compounds containing both phosphorous and nitrogen can display enhanced flame retardancy when compared to similar compounds containing phosphorous alone. In addition, these materials yield relatively minor amounts of toxic combustion products in fire situations. Therefore, the properties of organic polymers can be modified to significantly improve their fire resistance, ionic conductivity and biological compatibility by incorporating small amounts of specially modified eco-friendly phosphazene.[13–15] Hence, this makes phosphazenes particularly good candidates for the development of fire resistant eco-friendly materials in electrical and electronic applications.

With this in mind, the present study is focused on the synthesis and characterization of ATCP/FRHA/Bz-Ep composites for flame retardant applications. The improved thermal properties of ATCP/FRHA/Bz-Ep composites were confirmed by TGA and DSC techniques. The flame retardant properties of synthesized composites were studied by UL-94 test, LOI and cone calorimetry measurements. Furthermore, the dielectric and hydrophobic nature of the composites are determined by BDS and contact angle measurements, respectively. From these results, it was concluded that the presence of N, P and silica (three in one) material can promote thermal, flame retardant, dielectric (low k) and hydrophobic properties.

Methods and materials

Hexachlorocyclotriphosphazene (CP) and 3-aminopropyltrimethoxysilane (3-APTMS) (99%) were purchased from Sigma Aldrich, India. Diglycidyl ether of bisphenol-A epoxy resin (LY556) (DGEBA) was purchased from Ciba-Geigy Ltd, India. 4-Acetamido phenol, bisphenol-A, triethylamine, potassium carbonate, aniline, sodium hydroxide, paraformaldehyde and other solvents (AR grade) were purchased from SRL Chemicals, India.

Synthesis of hexa(acetamidophenyl)cyclotriphosphazene (CPAC)

A mixture of 4-acetamido phenol (15.65 g, 0.1035 mol) and K_2CO_3 (21.09 g, 0.15824 mol) in dry acetone (200 ml) was agitated at room temperature for 30 minutes. To this mixture, hexachlorocyclotriphosphazene (CP) (5 g, 0.0143 mol) was added and refluxed at 60 °C for 4 days. The resulting product was then cooled to room temperature and filtered. The crude product (CPAC) was further purified using hexane and dried in a vacuum oven at 50 °C for 2 h. The yield of the product and melting point were found to be 62.95% and 252–255 °C, respectively.

Synthesis of amine-terminated cyclophosphazene (ATCP)

A mixture of hexa(acetamidophenyl)cyclotriphosphazene (CPAC) (9 g), methanol (180 ml) and sulfuric acid (108 ml) was refluxed for 4 h at 80 °C and then cooled to room temperature followed by the dropwise addition of ammonia in an ice bath until the pH reached 8. The resultant grey solid product (Fig. 1) was filtered, washed with excess water and dried in vacuum at 50 °C for 48 h. The yield of the product and melting point were found to be 90% and 172–174 °C, respectively.

Preparation of rice husk ash

Rice husk was collected from a local rice mill in Tamil Nadu, India, and washed several times with de-ionized water. It was dried in sunlight for 7 days. The dried rice husk was burned in open air. After burning, the residue was crushed to obtain rice husk ash (RHA). The crushed rice husk ash (40 g) was immersed in 1 M HCl (1 liter) solutions for 4 h and then washed repeatedly with de-ionized water and dried in an oven at 110 °C for 2 days. Rice husk ash was calcined (in a ceramic crucible) at 350 °C for 3 h and 600 °C for 4 h in a muffle furnace. The resultant rice husk ash was white in color and was stored for further use.

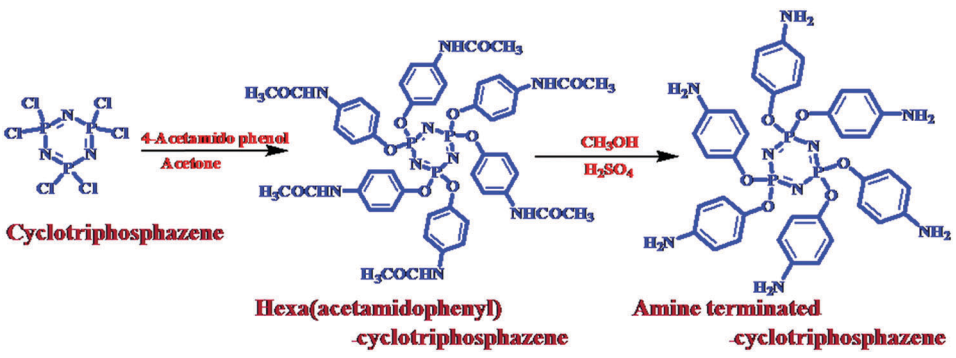

Fig. 1 Synthesis of amine-terminated cyclotriphosphazene.

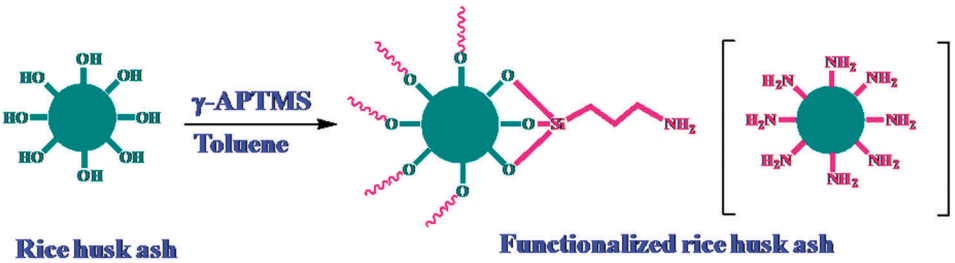

Fig. 2 Synthesis of functionalized rice husk ash.

Functionalization of RHA

RHA silica is functionalized with 3-aminopropyltrimethoxysilane (3-APTMS) according to the reported method.[16] 50 g of rice husk ash was mixed with 400 ml of dried toluene. The mixture was refluxed under a nitrogen atmosphere for 2 h and then 20 ml of 3-aminopropyltrimethoxysilane (3-APTMS) was slowly added. Finally, the resultant product was then filtered, washed with ethanol and dichloromethane several times and dried at 25 °C for 24 h. The resultant functionalized rice husk ash (FRHA) was stored for further use (Fig. 2).

Synthesis of flame retardant composites

According to our previous report, 15 wt% of CPA (hexa(aminophenyl)cyclotriphosphazene) is more effective than the other weight percentage ratios used.[17,18] Hence, DGEBA epoxy resin and benzoxazine (Bz)[19] were mixed with 15 wt% of amine-terminated cyclotriphosphazene and various weight percentages (1, 3 and 5%) of functionalized rice husk ash (Table 1). The resultant reaction mixture was agitated for 5 h using a mechanical stirrer. The amine-terminated cyclophosphazene, silane functionalized rice husk ash, benzoxazine and epoxy material (ATCP/FRHA/Bz-Ep) composites (Fig. 3) were thoroughly mixed and then cured using preheated moulds at 120 °C for 1 h, 180 °C for 1 h and 250 °C for 2 h in order to get ATCP/FRHA/Bz-Ep composites.

Characterization

FT-IR spectra were obtained on a Perkin Elmer 6× spectrometer. The surface morphologies of the samples were examined using a scanning electron microscope (SEM; JEOL JSM Model 6360). X-ray diffraction patterns were acquired at 25 °C using a Rich Seifert, Model-3000 X-ray powder diffractometer (monitoring the diffraction angle at 2θ from 10° to 70°). Thermogravimetric analysis (TGA) was performed on a Netzsch STA 409 thermogravimetric analyzer under a continuous flow of nitrogen (20 ml min^{-1}) at a heating rate of 10 °C min^{-1}. Differential scanning calorimetric (DSC) analysis was performed on a Netzsch DSC-200. The samples (each about 10 mg) were heated from 25 °C to 500 °C and the thermograms were recorded at a heating rate of 10 °C min^{-1}. The dielectric constant and dielectric loss of the samples were measured using a broad band dielectric spectrometer (BDS-NOVOCONTROL Technologies, Germany) at 35 °C in the frequency range from 1 Hz to 2 MHz. Contact angle measurements were carried out by a goniometer using the sessile drop method. Before measuring the contact angle, the samples should be dried at 60 °C in a vacuum oven for 24 h. The vertical burning tests were carried out using a UL-94 vertical flame chamber instrument with a sample dimension of 130 × 13 × 3 mm according to ASTM D3801. The limiting oxygen index (LOI) was analyzed with a sample dimension of 150 × 37.5 × 12 mm using an Atlas HVUL2 according to ASTM D2863. The cone calorimetry tests were conducted following the ISO 5660 procedures on a cone calorimeter (Fire Testing Technology Ltd). Specimens [dimensions: 100 × 100 × 2.9 (±0.1) mm^3] were irradiated with a heat flow of 50 kW m^{-2}. From this analysis, the time to ignition (TTI), heat release rate (HRR), total heat release (THR), total smoke production (TSP), char residues, and CO/CO_2 emission rate ratio can be acquired.

Table 1 Preparation of amine-terminated cyclophosphazene and functionalized rice husk ash based flame retardant (ATCP/FRHA/Ep-Bz) composites

Sample code	ATCP (g)	FRHA (g)	Bz (g)	Ep (g)	THF (ml)
Bz–Ep		—	50	50	20
ATCP/Bz-Ep	15	—	42.5	42.5	20
ATCP/FRHA(1%)/Bz-Ep	15	1	42	42	20
ATCP/FRHA(3%)/Bz-Ep	15	3	41	41	20
ATCP/FRHA(5%)/Bz-Ep	15	5	40	40	20

Results and discussions

Structural characterization

The two broad bands observed at 3438 and 3338 cm^{-1} correspond to $-NH_2$ stretching vibrations, in fact they also ascertain the presence of the amine group in the ATCP material (Fig. 4). The peaks observed at 3043 and 2925 cm^{-1} correspond to ring C–H stretching vibrations. The aromatic C–C stretching vibrations were noticed at 1507 and 1621 cm^{-1}. The characteristic stretching vibrations of P–O–Ph, P–N–P and P–O–C were seen at 1256, 1178 and 952 cm^{-1}, respectively. The aromatic C–H bending vibrations appeared at 832 and 695 cm^{-1}.

In the ^{13}C NMR spectrum (Fig. 5a), the presence of aromatic carbon was confirmed by the peaks observed at 111.5 and 120.3 ppm. From the ^{1}H NMR spectrum (Fig. 5b), the presence of aromatic protons in ATCP was confirmed by the appearance of the peaks at 6.52 and 7.2 ppm. The presence of NH_2 protons was confirmed by the peak at 2.3 ppm. The appearance of the peak at 30.1 confirms the presence of carbon that was attached to a NH_2 group in the ATCP material. A single peak appearing at

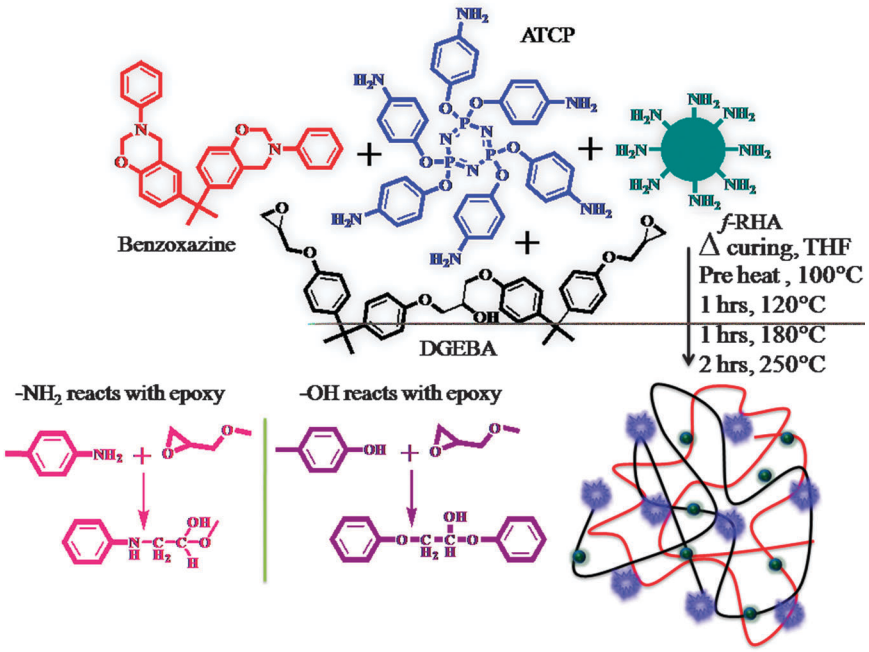

Fig. 3 Proposed schematic of amine-terminated cyclophosphazene and functionalized rice husk ash reinforced benzoxazine blend epoxy composites.

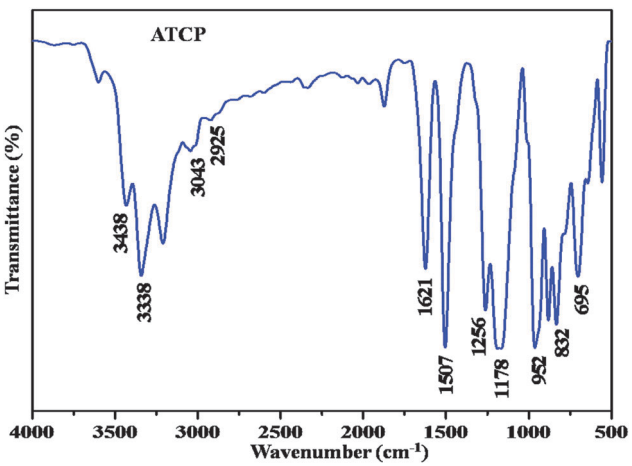

Fig. 4 FT-IR spectrum of amine-terminated cyclophosphazene (ATCP).

10.1 ppm in the ^{31}P NMR spectrum (Fig. 5c) confirms the presence of phosphorous in the ATCP material.

Fig. 6 shows the FT-IR spectra of rice husk ash and functionalized rice husk ash. The peak observed at 3473 cm^{-1} indicates the presence of both hydrogen bonded –OH and Si–OH groups. The Si–OH stretching vibration appears due to both the silanol group and adsorbed water on the surface.[20] Similarly, the peak observed at 2937 cm^{-1} indicates the presence of $-CH_2$ stretching vibration. The peaks appearing at 1095 and 800–798 cm^{-1} confirm the presence of the Si–O–Si bond. Thus, these results show that the aminopropyl groups have become an integral part of RHA and are covalently bonded with the RHA material.

The FT-IR spectra of Bz–Ep, ATCP/Bz-Ep, ATCP/FRHA(1%)/Bz-Ep, ATCP/FRHA(3%)/Bz-Ep and ATCP/FRHA(5%)/Bz-Ep composites are shown in Fig. 7. The peak observed at 3433 cm^{-1} corresponds to OH stretching vibrations. The stretching bands observed at 2961 and 2865 cm^{-1} correspond to C–H stretching vibrations. The peak observed at 1041 cm^{-1} confirms the presence of C–O stretching vibrations. The aromatic C–C stretching vibrations were observed at 1514 and 1613 cm^{-1}. The characteristic stretching vibrations of P–O–Ph, P–N–P and P–O–C were observed at 1257 cm^{-1}, 1186 cm^{-1} and 946 cm^{-1}, respectively. The peak at 827 cm^{-1} confirms the presence of aromatic C–H bending vibrations. The Si–O–Si peak was observed at 1000–1130 cm^{-1}. The abovementioned results confirm the complete curing of ATCP/FRHA/Bz-Ep composites.

Surface morphology

From the SEM image of the Bz–Ep composite [Fig. 8(a)], it was noticed that the synthesized composite material has a homogeneous glassy microstructure.

Furthermore, the ATCP/Bz-Ep/FRHA composite [Fig. 8(b–e)] shows a platelet-like surface morphology and exhibits the non-phase separated homogeneous morphology owing to cross-linking between the benzoxazine-based epoxy resin with amine-terminated cyclophosphazene and the functionalized rice husk ash materials.

X-ray diffraction analysis

The X-ray diffraction studies were used to ascertain the structural modification of Bz–Ep, ATCP/Bz-Ep, ATCP/FRHA(1%)/Bz-Ep, ATCP/FRHA(3%)/Bz-Ep and ATCP/FRHA(5%)/Bz-Ep composites. The resultant XRD patterns of synthesized composites are shown in Fig. 9. The cured composites have almost similar prominent peaks at an angle of about 17.95°, which is a characteristic of amorphous[21,22] composites corresponding to the interaction at a d spacing of 4.9 Å calculated from the Bragg

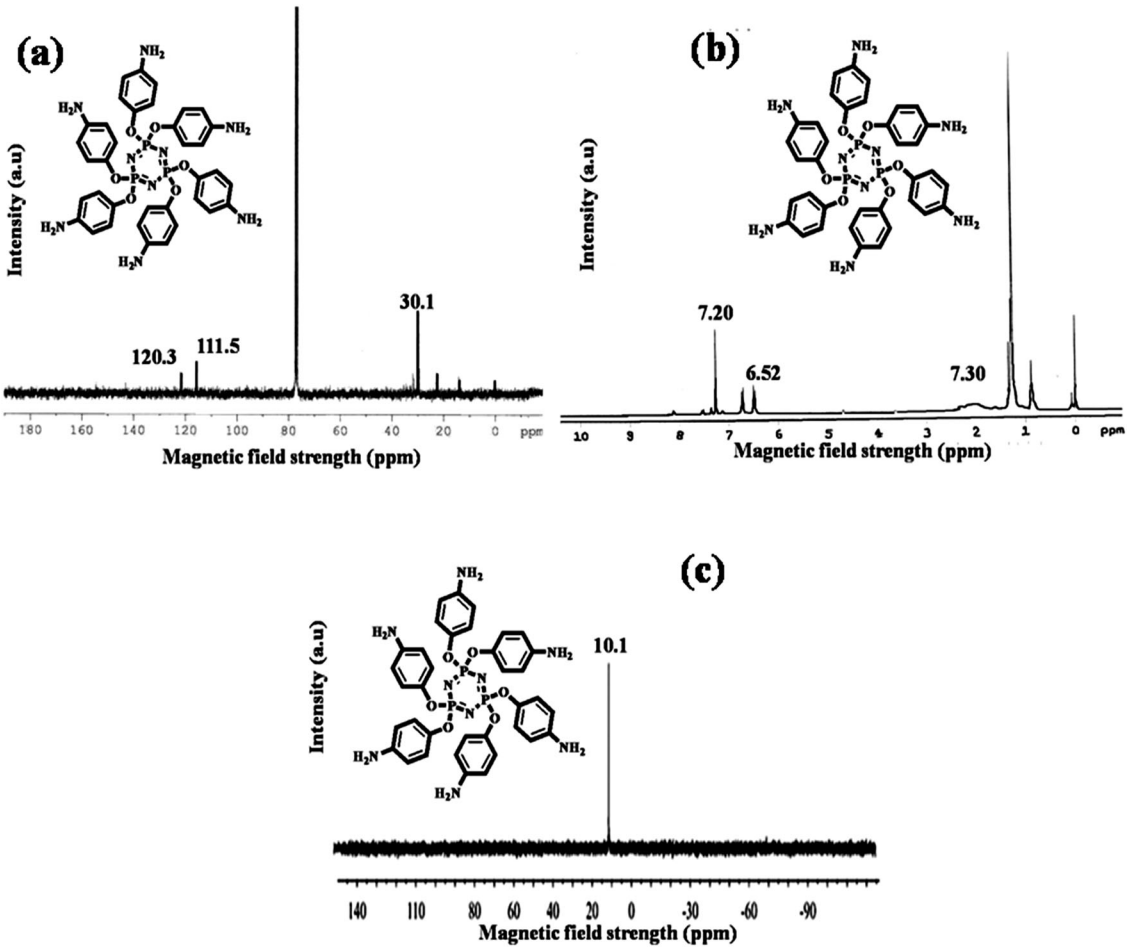

Fig. 5 (a) ^{13}C NMR, (b) ^{1}H NMR and (c) ^{31}P NMR spectra of synthesized ATCP.

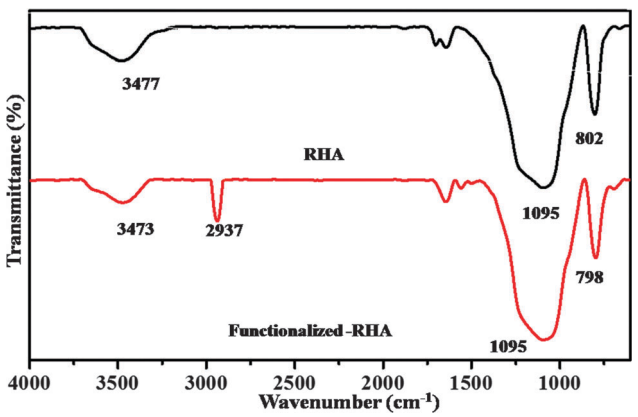

Fig. 6 FT-IR spectra of rice husk ash and functionalized rice husk ash materials.

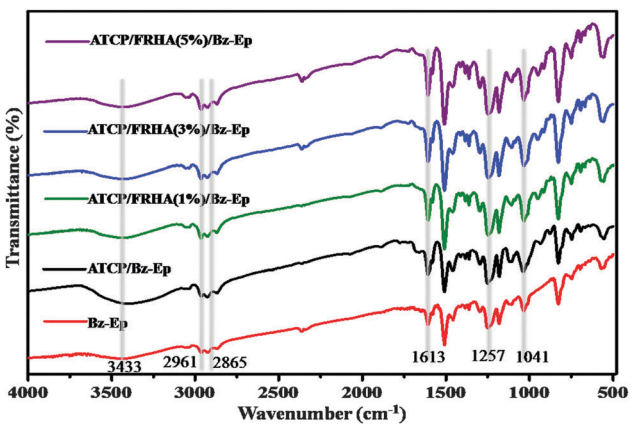

Fig. 7 FT-IR spectra of Bz–Ep, ATCP/Bz-Ep, ATCP/FRHA(1%)/Ep-Bz, ATCP/FRHA(3%)/Bz-Ep and ATCP/FRHA(5%)/Bz-Ep flame retardant composites.

equation ($\lambda = 2d\sin\theta$). Hence, the XRD studies confirm the complete incorporation of flame retardant additive-like ATCP and FRHA materials in the Bz–Ep blends.

Contact angle measurements

The wettabilities of Bz–Ep, ATCP/Bz-Ep, ATCP/FRHA(1%)/Bz-Ep, ATCP/FRHA(3%)/Bz-Ep and ATCP/FRHA(5%)/Bz-Ep composites were determined through contact angle measurements using a goniometer. The surface contact angles were measured with 5 μl of water as the probe liquid and the results are presented in Fig. 10. The values of the contact angles of Bz–Ep, ATCP/Ep-Ep, ATCP/FRHA(1%)/Bz-Ep, ATCP/FRHA(3%)/Bz-Ep and ATCP/FRHA(5%)/Bz-Ep composites are 68°, 82°, 86°, 98°

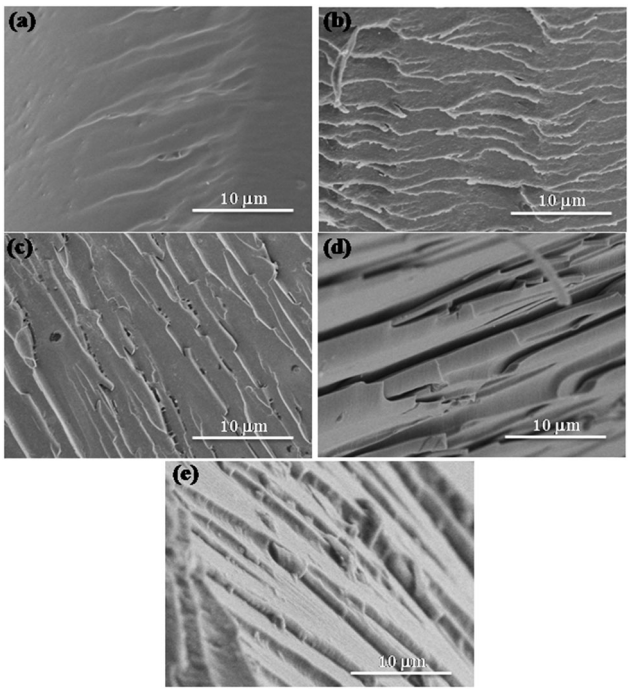

Fig. 8 Fracture morphology of (a) Bz–Ep, (b) ATCP/Bz-Ep, (c) ATCP/FRHA(1%)/Bz-Ep, (d) ATCP/FRHA(3%)/Bz-Ep and (e) ATCP/FRHA(5%)/Bz-Ep composites.

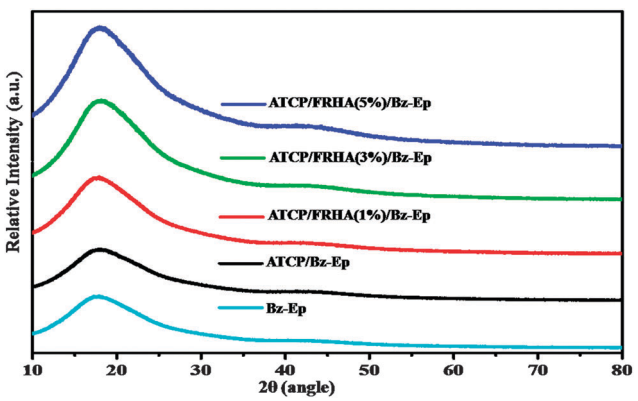

Fig. 9 XRD analysis of Bz–Ep, ATCP/Bz-Ep, ATCP/FRHA(1%)/Bz-Ep, ATCP/FRHA(3%)/Bz-Ep and ATCP/FRHA(5%)/Bz-Ep flame retardant composites.

and 106°, respectively. From the results, it was noticed that the hydrophobic nature can be increased with the addition of phosphazene and various percentages of functionalized rice husk ash into the Bz–Ep composite. This is due to the less polar nature of the Si–O–Si linkages in the network system, which increases the hydrophobic nature of the resulting hybrid systems.

Dielectric properties

The dielectric constants with respect to the applied AC frequencies ranging from 1 MHz to 20 MHz are presented in Fig. 11. The obtained dielectric constant and dielectric loss values are

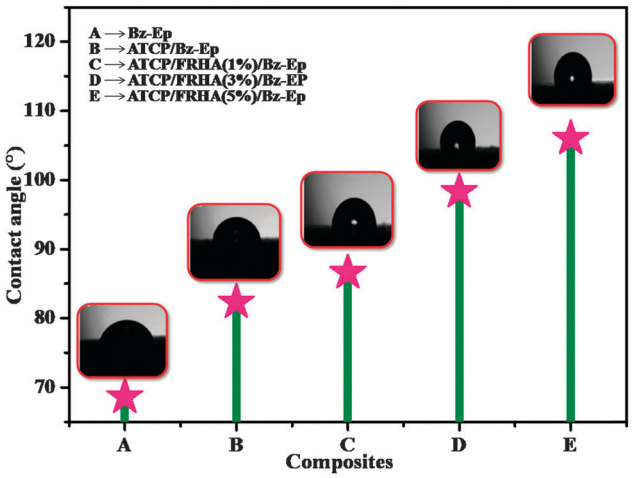

Fig. 10 Contact angle measurements of Bz–Ep, ATCP/Bz-Ep, ATCP/FRHA(1%)/Bz-Ep, ATCP/FRHA(3%)/Bz-Ep and ATCP/FRHA(5%)/Bz-Ep flame retardant composites.

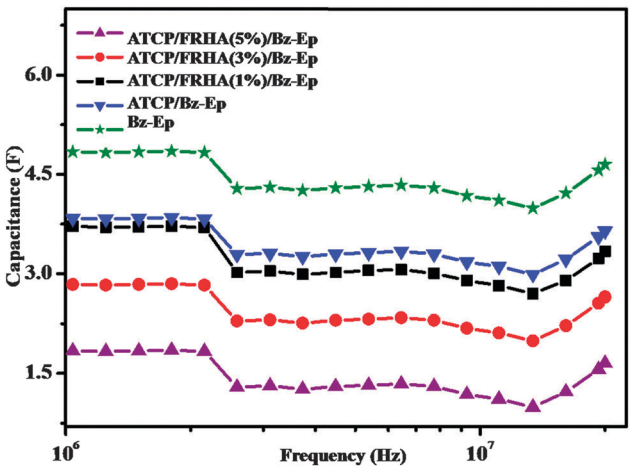

Fig. 11 Dielectric constant of Bz–Ep, ATCP/Bz-Ep, ATCP/FRHA(1%)/Bz-Ep, ATCP/FRHA(3%)/Bz-Ep and ATCP/FRHA(5%)/Bz-Ep composites.

given in Table 2. From Fig. 11, it was noticed that the ATCP/FRHA(5%)/Bz-Ep hybrid has a lower value of dielectric constant (~1.62) than that of the Bz–Ep (~4.63) composite.

Furthermore, the polybenzoxazine network structure constructed *via* multiple cross-links and subsequent hydrogen bonding (–OH···O inter- and –OH···N intramolecular hydrogen

Table 2 The dielectric constant, dielectric loss, charge transfer resistance and contact angle values of flame retardant composites

Sample name	Dielectric constant	Dielectric loss	Charge transfer resistance (Ω)	Contact angle value
Bz–Ep	4.63	0.215	5.27×10^9	68°
ATCP/Bz-Ep	3.64	0.194	5.95×10^9	82°
ATCP/FRHA(1%)/Bz-Ep	3.32	0.173	7.11×10^9	86°
ATCP/FRHA(3%)/Bz-Ep	2.65	0.135	8.52×10^9	98°
ATCP/FRHA(5%)/Bz-Ep	1.62	0.091	9.55×10^9	106°

bonds) may be the reason for the observed dielectric features.[23–25] This inter- and intramolecular hydrogen bonding can influence the change in polarization throughout the polymer network. In addition, the intermolecular hydrogen bonding can obviously enhance the polarization and dielectric constant, whereas the intramolecular hydrogen bonding contributes toward reducing the dielectric constant.[25] Furthermore, the composites have a higher volume fraction of intramolecular hydrogen bonding, which can help reduce the interfacial polarizability and hence the dielectric constant values are reduced. In addition to that ATCP/FRHA/Bz-Ep hybrid composites have siloxane and a highly cross-linked structure, which can also decrease the dielectric constant and dielectric loss.

The dielectric loss is another important factor to apply the material for commercial microwave electronic devices. An almost negligible dielectric loss is desirable for practical applications. Frequency-dependent dielectric loss spectra of Bz–Ep, ATCP/Bz-Ep, ATCP/FRHA(1%)/Bz-Ep, ATCP/FRHA(3%)/Bz-Ep and ATCP/FRHA(5%)/Bz-Ep composites are shown in Fig. 12 and their resulting values are presented in Table 2. Similar to the dielectric constant, the values of dielectric loss also follow the decreasing trend from Bz–Ep to ATCP/FRHA/Bz-Ep and their results are presented in Table 2. ATCP/FRHA/Bz-Ep systems have low dielectric constants, which is due to high cross-linking densities, siloxane structure, intramolecular hydrogen bonding and reduced surface free energy that promotes the hydrophobic nature[26,27] of the composites.

Apart from this, the dielectric constants mainly depend on the polarizability of the materials, and the materials with less polar functional groups favour a low k value. Furthermore, the incorporation of the less polar Si–O–Si containing rice husk ash also contributes to reduce the dielectric constant. In addition, the cross-links in ATCP/FRHA/Bz-Ep maintain sufficient distance between the matrixes, which can significantly reduce the interfacial polarization that results in a very low k value for the hybrid polymer system. The phenomena such as less polar functional groups, large volume fraction of intramolecular hydrogen bonds,

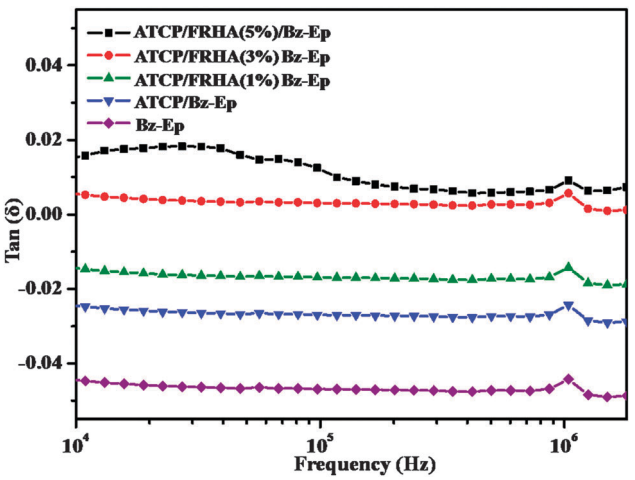

Fig. 12 Dielectric loss of Bz–Ep, ATCP/Bz-Ep, ATCP/FRHA(1%)/Bz-Ep, ATCP/FRHA(3%)/Bz-Ep and ATCP/FRHA(5%)/Bz-Ep composites.

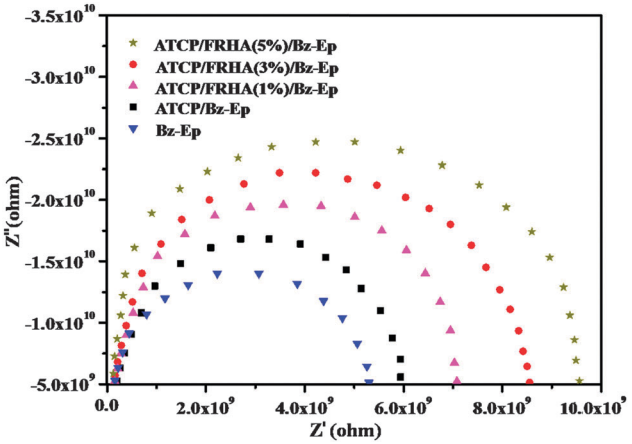

Fig. 13 Nyquist plot of Bz–Ep, ATCP/Bz-Ep, ATCP/FRHA(1%)/Bz-Ep, ATCP/FRHA(3%)/Bz-Ep and ATCP/FRHA(5%)/Bz-Ep flame retardant composites.

and low surface free energy are attributed to the low dielectric constant value (1.62 δ) with a high thermal stability as well as flame retardant ability for the ATCP/FRHA/Bz-Ep composites. Thus, the resultant ATCP/FRHA(5%)/Bz-Ep composite has a low k value, which can be used for high performance dielectric applications.

Impedance measurements were used to assess the dielectric behaviour of the polymer composites. From the Nyquist plot (Fig. 13), typical capacitance response was observed with semicircles for Bz–Ep, ATCP/Bz-Ep, ATCP/FRHA(1%)/Bz-Ep, ATCP/FRHA(3%)/Bz-Ep and ATCP/FRHA(5%)/Bz-Ep composites. The large semicircle is related to high charge transfer resistance (R_{ct}) and constant phase element (CPE_2). The decreased size of the semicircle indicates lower electrical resistivity due to the creation of conductive paths. This technique is based on the consideration of a linear electrical behaviour of the system under study. However, it has been reported that the polymeric composites can also show a non-linear electrical behaviour.[28,29] From this plot, it is seen that the charge transfer resistance values are 5.27×10^9, 5.95×10^9, 7.11×10^9, 8.52×10^9 and 9.55×10^9 Ω for Bz–Ep, ATCP/Bz-Ep, ATCP/FRHA(1%)/Bz-Ep, ATCP/FRHA(3%)/Bz-Ep and ATCP/FRHA(5%)/Bz-Ep composites, respectively (Table 2). From the results, it was concluded that the ATCP/FRHA(5%)/Bz-Ep composites exhibit higher charge transfer resistances (R_{ct}) than the Bz–Ep composite.

Thermal properties

The glass transition temperature (T_g) of Bz–Ep, ATCP/Bz-Ep, ATCP/FRHA(1%)/Bz-Ep, ATCP/FRHA(3%)/Bz-Ep and ATCP/FRHA(5%)/Bz-Ep composites were determined by DSC measurements and the data obtained are listed in Table 3. The Bz–Ep matrix shows a lower T_g value than that of the other composites (Fig. 14). The increased value of T_g for ATCP/FRHA/Bz-Ep composites is may be due to the presence of high cross-linking density among the amine-terminated cyclophosphazene functionalized rice husk ash (which exists as a thermally stable Si–O–Si skeleton in the composite) and benzoxazine-based epoxy composites.[30] Therefore, the introduction of rigid groups into the

Table 3 Thermal properties of Bz–Ep, ATCP/Bz-Ep, ATCP/FRHA(1%)/Bz-Ep, ATCP/FRHA(3%)/Bz-Ep and ATCP/FRHA(5%)/Bz-Ep composites

		TGA in nitrogen atmosphere			TGA in air		
Thermoset sample	T_g (°C)	T_{onset}[a] (°C)	T_{max}[b] (°C)	Char yield at 800 °C (wt%)	T_{onset}[a] (°C)	T_{max}[b] (°C)	Char yield at 800 °C (wt%)
Bz–Ep	211	318	370	22.57	313	367	20.84
ATCP/Bz-Ep	218	322	374	29.47	317	370	24.97
ATCP/FRHA(1%)/Bz-Ep	223	328	378	30.42	325	374	28.64
ATCP/FRHA(3%)/Bz-Ep	233	333	385	39.46	329	382	34.54
ATCP/FRHA(5%)/Bz-Ep	240	338	393	44.25	334	390	41.20

[a] The onset decomposition temperature at which the thermoset undergoes 5 wt% of weight loss. [b] The characteristic temperature at which maximum rate of weight loss of 40 wt% occurs.

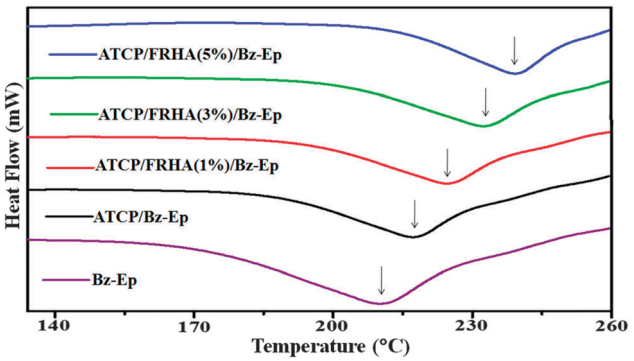

Fig. 14 DSC analysis of Bz–Ep, ATCP/Bz-Ep, ATCP/FRHA(1%)/Bz-Ep, ATCP/FRHA(3%)/Bz-Ep and ATCP/FRHA(5%)/Bz-Ep flame retardant composites.

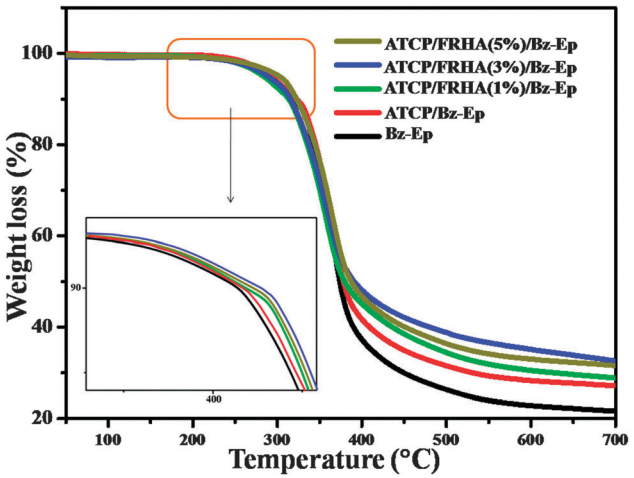

Fig. 15 TGA analysis for Bz–Ep, ATCP/Bz-Ep, ATCP/FRHA(1%)/Bz-Ep, ATCP/FRHA(3%)/Bz-Ep and ATCP/FRHA(5%)/Bz-Ep flame retardant composites under a nitrogen atmosphere.

backbone of a benzoxazine-based epoxy composite can increase the T_g value of the resulting cured composite.

Thermogravimetric analysis (TGA) technique is another powerful tool to evaluate the thermal stability of composites. TGA traces of cured benzoxazine-based epoxy composites can provide important information about their thermal stability and thermal degradation behavior. Fig. 15 and 16 show the TGA thermograms and DTG curves of hybrid composites in the nitrogen atmosphere and the results are presented in Table 3. The 5% weight loss temperature of Bz–Ep, ATCP/Bz-Ep, ATCP/FRHA(1%)Bz-Ep, ATCP/FRHA(3%)/Bz-Ep and ATCP/FRHA(5%)/Bz-Ep composites were 318, 322, 328, 333 and 338 °C, respectively. The variation in degradation values observed is due to the presence of phosphorous- and nitrogen-containing amine-terminated cyclophosphazene and silicon-containing functionalized rice husk ash in the epoxy composites. Similar trends have also been observed for maximum weight loss (Fig. 16) of the composites. Furthermore, it was noticed that the presence of amine-terminated cyclophosphazene and increasing weight percentages of functionalized rice husk ash can increase the thermal stability of the resulting composites. The decomposition temperature of phosphorus-containing composites is higher than that of the conventional epoxy matrices, which is due to the presence of P–C bonds, since the P–C bond has a higher thermal stability than the C–C bond.[31] The major weight loss observed above 300 °C is associated with the decomposition of the polymer network and finally yields a residual char at 800 °C.

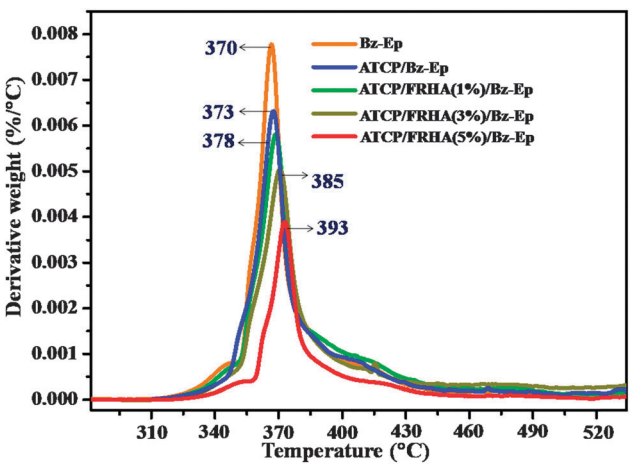

Fig. 16 DTG curve of Bz–Ep, ATCP/Bz-Ep, ATCP/FRHA(1%)/Bz-Ep, ATCP/FRHA(3%)/Bz-Ep and ATCP/FRHA(5%)/Bz-Ep flame retardant composites.

From Table 3, it can be seen that the value of char yield increases with increase in wt% of reinforcement, which is due to the presence of phosphorous, nitrogen and (1%, 3% and 5%) silicon in the composite systems. A relatively higher char yield is obtained for the ATCP/Bz-Ep/FRHA(5%) composite compared to that of the Bz–Ep composite. Furthermore, the higher char

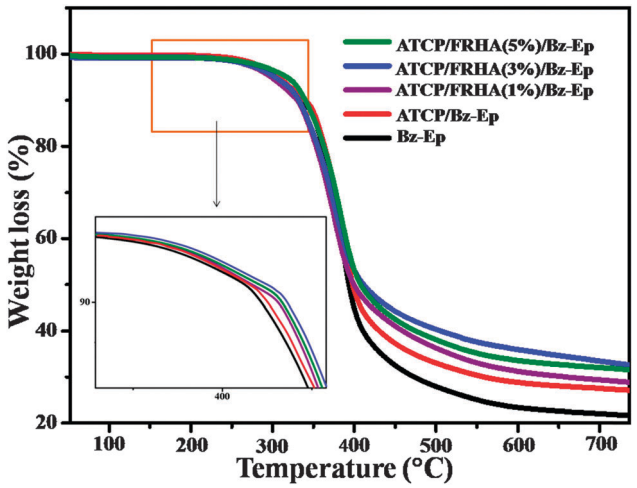

Fig. 17 TGA curves of Bz–Ep, ATCP/Bz-Ep, ATCP/FRHA(1%)/Bz-Ep, ATCP/FRHA(3%)/Bz-Ep and ATCP/FRHA(5%)/Bz-Ep flame retardant composites in air.

yield confirms higher flame retardant properties. Hence, the introduction of phosphorous, nitrogen and silicon into the modified Bz–Ep shows better flame retardancy than that of a pure Bz–Ep matrix. Data obtained from thermal analysis indicates that ATCP/FRHA/Bz-Ep composites exhibit higher thermal stability and better flame retardancy than those of a benzoxazine-based epoxy matrix.

The TGA curves of Bz–Ep, ATCP/Bz-Ep, ATCP/FRHA(1%)/Bz-Ep, ATCP/FRHA(3%)/Bz-Ep and ATCP/FRHA(5%)/Bz-Ep flame retardant composites in an air atmosphere are shown in Fig. 17. The decomposition processes of flame retardant composites in air were similar to those in an N_2 atmosphere.

Flame retardant properties

The flammability characteristics of the composites were evaluated by UL-94 vertical burning experiment; LOI values and their results are tabulated in Table 4. From the results, it was noticed that the prepared composites achieved the V-0 classification except the Bz–Ep composite and their corresponding LOI values increased from 28% to 51%. On this basis, it was concluded that the ATCP- and FRHA-containing Bz–Ep composites have a virtually non-flammable nature. Such good inherent flame retardancy is ascribed to the presence of a unique combination of phosphorous, nitrogen and siloxane networks in ATCP and rice husk ash incorporated Bz–Ep materials. The occurrence of the abovementioned inorganic elements can promote the formation of intumescent carbonaceous char, which enhances flame retardancy in the form of a condensed phase. Such a category of a flame retarding mechanism is well known as an intumescent mechanism. In this mechanism, an organic material can swell when exposed to fire or heat to form a foamed mass usually carbonaceous in the condensed phase, promoting char formation on the surface as a barrier to inhibit gaseous products from diffusing to the flame and shielding the polymer surface from heat.

Cone calorimetry is often used to evaluate the fire resistance behaviour of materials and its measurements provide several useful burning parameters.[32–37] Fig. 18 and 19 show time to ignition (TTI), the heat release rate (HRR), total heat release rate (THR), total smoke production (TSP), carbon monoxide production (COP), and smoke production rate (SPR) for Bz–Ep, ATCP/Bz-Ep, ATCP/FRHA(1%)/Bz-Ep, ATCP/FRHA(3%)/Bz-Ep and ATCP/FRHA(5%)/Bz-Ep composites. Time to ignition was used to determine the influence on ignitability, which can be measured from the onset of the HRR curve (Table 4). TTI showed clear differences in the ignition behaviour among the composite materials developed, and TTI of the cured ATCP/FRHA(5%)/Bz-Ep system was smaller than that of Bz–Ep thermosets, which may be due to the presence of flame retarded ATCP and FRHA (Table 4) in the composite materials.

HRR is the measurement of heat release per unit surface area of a burning specimen. This is considered as a typical case for thin non-charring materials. The ATCP/FRHA/Bz-Ep composites show significant flame retardant effects with a drastic decrease in peak heat release rate (PHRR) from 713 to 289 kW m^{-2}. The combination of both amine-terminated cyclophosphazene (ATCP) and functionalized rice husk ash (FRHA) leads to the improvement in the flame retardant performance of the materials when compared with Bz–Ep and ATCP/Bz-Ep composites.

The peak originates from the full heat releasing of the insulating layer on the surface of the polymer composite. Herein, the phosphorus groups form an insulating protective layer, which prevents the volatiles from transferring to the surface of the material and thus increases the thermal stability of the char at higher temperatures. Furthermore, nitrogen in polymers can release non-flammable gases or decompose endothermically to cool the pyrolysis zone at the combustion surface,[38] and silicon in the FRHA is likely to form thermally stable silica that has a tendency to migrate onto the char surface, which serves as a protection layer to prevent the further degradation of char at high temperatures.[39,40]

Fig. 18(b) shows the total heat release (THR) curves of typical flame retarded composites. ATCP/FRHA(5%)/Bz-Ep shows the

Table 4 Cone calorimetry and UL-94 vertical burning test results of flame retardant composites

Sample names	UL-94 test	LOI value (%)	TTI (s)	PHRR (KW m^{-2})	THR (MJ m^{-2})	PCOP (g s^{-1})	PSPR (m^2 s^{-1})	TSP (m^2)
Bz–Ep	V-1	28	57	713	64	0.033	0.16	12.98
ATCP/Bz-Ep	V-0	34	52	610	58	0.025	0.13	11.33
ATCP/FRHA(1%)/Bz-Ep	V-0	39	48	435	51	0.021	0.10	8.77
ATCP/FRHA(3%)/Bz-Ep	V-0	45	45	374	43	0.017	0.07	7.36
ATCP/FRHA(5%)/Bz-Ep	V-0	51	40	289	31	0.013	0.05	5.52

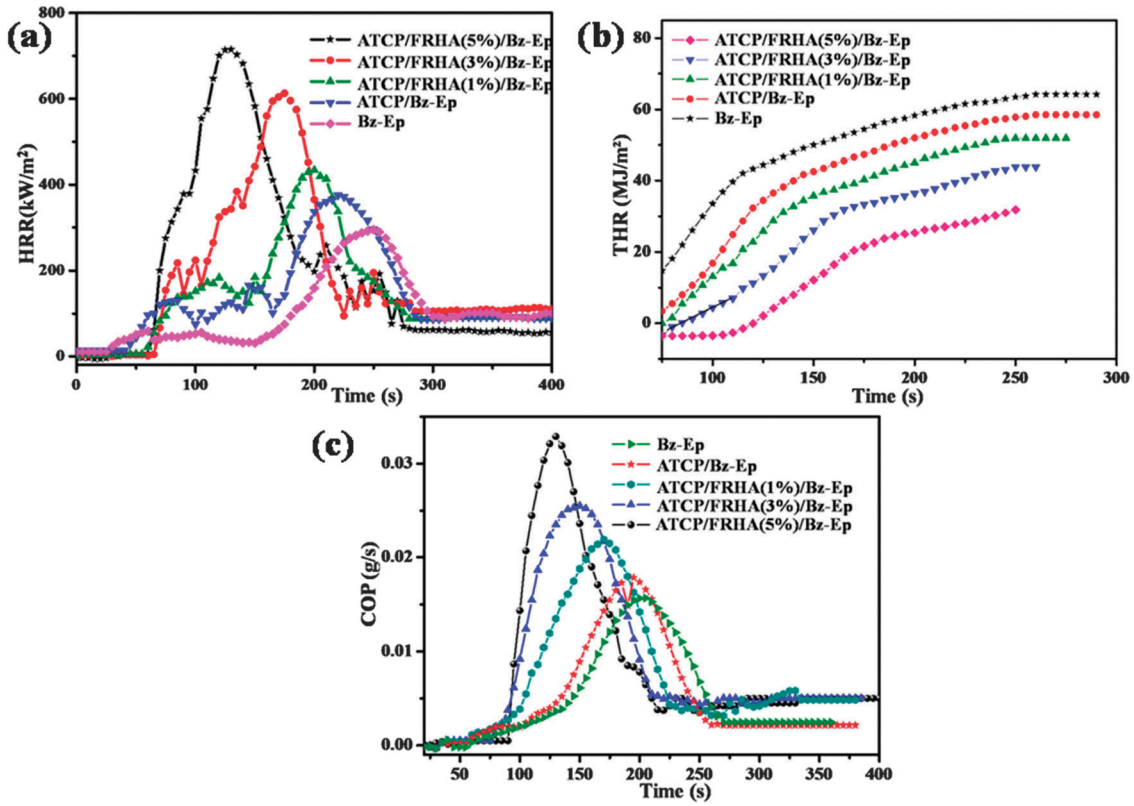

Fig. 18 (a) Heat release rate (HRR), (b) total heat release rate (THR) and (c) carbon monoxide production (COP) of Bz–Ep, ATCP/Bz-Ep, ATCP/FRHA(1%)/Bz-Ep, ATCP/FRHA(3%)/Bz-Ep and ATCP/FRHA(5%)/Bz-Ep composites.

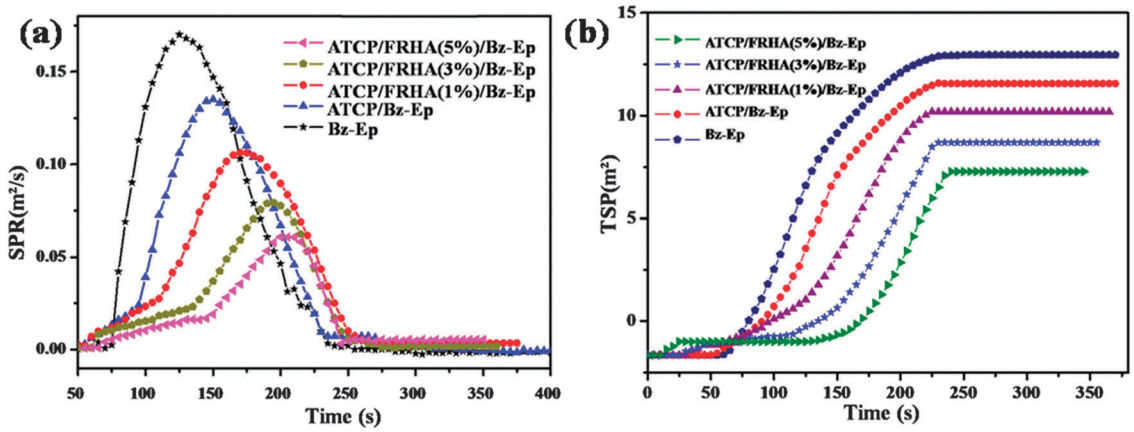

Fig. 19 (a) Smoke production rate (SPR) and (b) total smoke production (TSP) of Bz–Ep, ATCP/Bz-Ep, ATCP/FRHA(1%)/Bz-Ep, ATCP/FRHA(3%)/Bz-Ep and ATCP/FRHA(5%)/Bz-Ep flame retardant composites.

lowest THR value among all the flame retardant samples, which further evidences the good flame retardant performance. The decrease in THR value of the ATCP/FRHA(5%)/Bz-Ep composite indicates that a part of the polymer is not completely burnt. Hence, the compact protective layers on the surface serve as a thermal insulation layer that can inhibit polymer pyrolysis, which is the evolution of combustible gases to feed the flame, and act as a barrier to separate oxygen from the burning materials.[41]

The evolution of smoke is considered as another important parameter in the halogen-free flame retardant materials. The formation of CO in fires takes place at low temperatures in the early stage of fire development, which is primarily attributed to the incomplete combustion of the pyrolyzed polymer volatile products. When fire develops, higher temperatures favour the formation of CO_2, which is particularly dependent on oxygen availability to the fire.[42,43] Fig. 18(c) shows the CO releasing rate during the combustion of composites. It can be seen that the

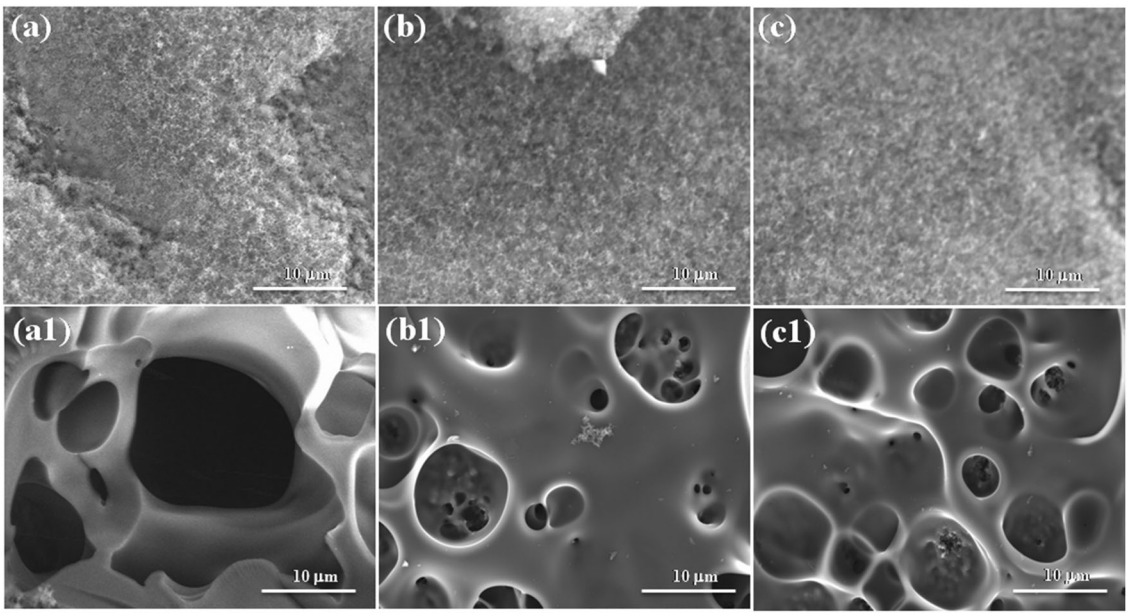

Fig. 20 Char morphology and inner layer morphology of (a) and (a1) Bz–Ep, (b) and (b1) ATCP/Bz-Ep and (c) and (c1) ATCP/FRHA(1%)/Bz-Ep flame retardant composites.

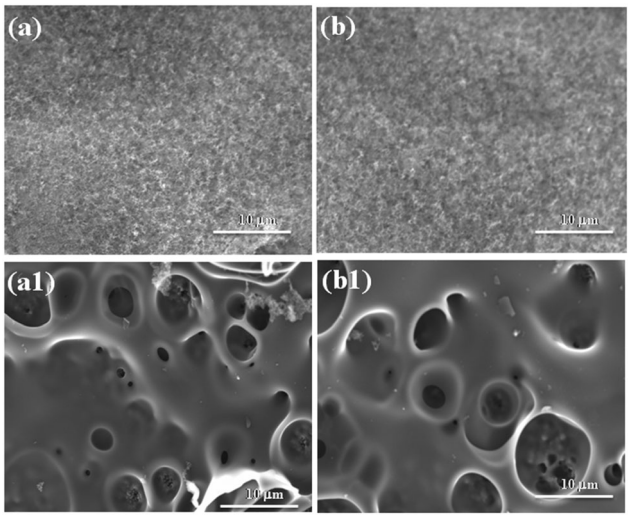

Fig. 21 Char morphology and inner layer morphology of (a) and (a1) ATCP/FRHA(3%)/Bz-Ep and (b) and (b1) ATCP/FRHA(5%)/Bz-Ep flame retardant composites.

CO productions of the flame retardant ATCP/FRHA(5%)/Bz-Ep sample are much lower than that of Bz–Ep composites during combustion.

Development of flame retardant materials with low-smoke polymers is a long-pursued target (Fig. 19(a)). The ATCP/FRHA(5%)/Bz-Ep sample has a much lower smoke production rate than that of other Bz–Ep composites. From the results, it was concluded that the accumulation of ATCP intumescent flame retardant together with FRHA near the regressing sample surface acts as not only as a heat insulation layer but also as a barrier that prevents the decomposed volatile products migrating to the sample surface.

Analysis of residual char

SEM micrographs of the outside and the inside features of the char obtained from the UL-94 test are shown in Fig. 20 and 21. The outside aspect of the char was observed to present a carbonaceous structure with a more compact and dense char layer, while the inside shows a multi-porous structure.

This result indicates the typical morphology associated with intumescent char formation. It was well known that the charring structure is one of the most important factors that determine the flame retardancy on the basis of SEM observation. The char layer looks rigid and compact with many integrated closed honeycomb pores in the inside structural features that could impart a temperature gradient to the char layer during combustion. Such a protective char layer can serve as a barrier against heat and oxygen diffusing items that protects the inside matrix. From the FE-SEM images, it was concluded that the use of cyclophosphazene and rice husk ash as a flame retardant material can lead to remarkably important flame retardant properties of the resultant composite materials.

Fig. 22 shows the FTIR spectra of the residual chars collected from the UL-94 test of Bz–Ep, ATCP/Bz-Ep, ATCP/FRHA(1%)/Bz-Ep, ATCP/FRHA(3%)/Bz-Ep and ATCP/FRHA(5%)/Bz-Ep. The peak observed at 3433 cm^{-1} corresponds to NH stretching vibrations. The peaks at 2961 and 2865 cm^{-1} correspond to C–H stretching vibrations. The peak observed at 1041 cm^{-1} confirms the presence of C–O stretching vibrations. The aromatic C–C stretching vibration was observed at 1514 cm^{-1}. The characteristic stretching vibrations observed at 1257 cm^{-1}, 1186 cm^{-1} and 946 cm^{-1} suggest that P–O–Ph, P–N–P and P–O–C bonds exist in the residual chars of all the tested thermosets. Furthermore, the peak observed between 1000 and 1130 cm^{-1} confirms the presence of the Si–O–Si bond. From the overall

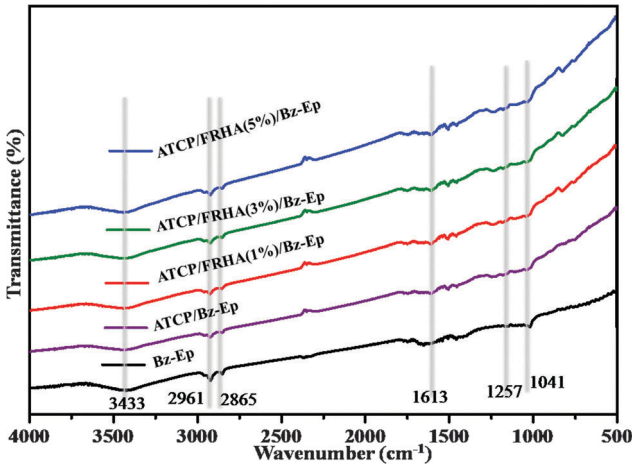

Fig. 22 FT-IR spectra of residues obtained from the UL-94 test.

results, it was concluded that synergistic effects occurred and strengthened with increasing FRHA mass ratio; this plays a very important role in the self-extinguishing performance of flame retardant ATCP/FRHA/Bz-Ep composites.

Fig. 23 shows the digital images of Bz–Ep, ATCP/Bz-Ep, ATCP/FRHA(1%)/Bz-Ep, ATCP/FRHA(3%)/Bz-Ep and ATCP/FRHA(5%)/Bz-Ep residues obtained after carrying out the vertical burning test. During the UL-94 vertical burning flame retardant test, all specimens were ignited with an alcohol lamp for 30 s. The amount and shape of residues formed during combustion were closely observed. Fig. 23(a) shows that a rare char was formed, which confirms the poor flame retardancy and melt dripping. Fig. 23(e) shows that a char layer was formed, and the thickness of this char layer increased with increasing mass ratio of ATCP and FRHA materials.

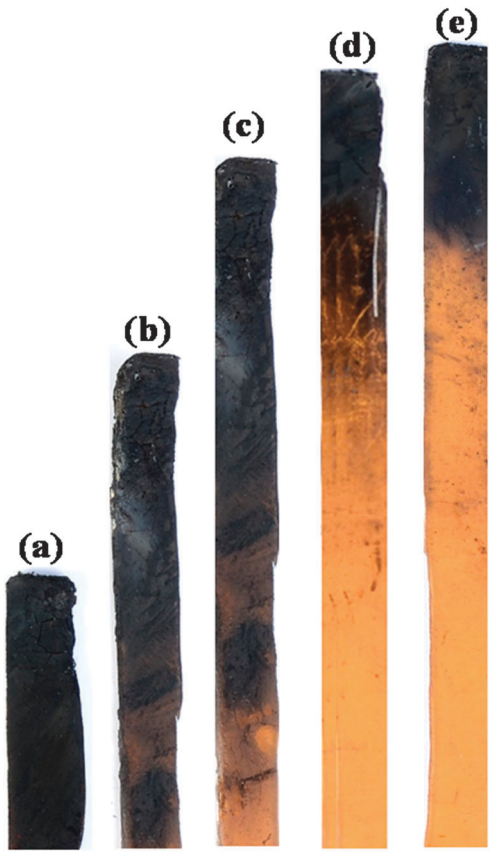

Fig. 23 Digital photos of (a) Bz–Ep, (b) ATCP/Bz-Ep, (c) ATCP/FRHA(1%)/Bz-Ep, (d) ATCP/FRHA(3%)/Bz-Ep and (e) ATCP/FRHA(5%)/Bz-E residue obtained after carrying out UL-94 vertical burning flame retardant test.

Conclusion

In this study, ATCP and FRHA were utilized together as a novel combined halogen-free flame retardant system to improve the flame retardance of benzoxazine blended epoxy composites. The addition of FRHA enhances both the flame retardance and dielectric properties of amine-terminated cyclophosphazene-reinforced benzoxazine-based epoxy matrix. The fracture surface exhibits a non-phase separated platelet-like homogeneous morphology. The dielectric constant and dielectric loss decreased due to the presence of intramolecular hydrogen bonding, high cross-linking density and orientation of the molecules. The improvement in the electrical resistivity was confirmed by Nyquist plots with high charge transfer resistance for the composite materials. The improved hydrophobic nature was confirmed by contact angle measurements. Furthermore, the introduction of a small amount of ATCP and FRHA were found to improve the degradation properties, leading to a compact and unbroken N, P and Si protective layer. Therefore, drastically depressed peak heat release rates were achieved. This novel flame retardant composite will open up new possibilities for high performance halogen-free flame retardant polymeric materials, which could be applied to micro-electronic devices.

Acknowledgements

The authors like to thank DST/Nanomission, New Delhi, India, for financial support to carry out this study and to establish Nanotech Research Lab through the grant no. SR/NM/NS-05/2011(G).

References

1 A. Riva, G. Camino, L. Fomperie and P. Amigouet, *Polym. Degrad. Stab.*, 2003, **82**, 341.
2 M. Fu and B. Qu, *Polym. Degrad. Stab.*, 2004, **85**, 633.
3 S. M. El-Sayed, H. M. Abdel Hamid and R. M. Radwan, *Radiat. Phys. Chem.*, 2004, **69**, 339.
4 J. Gu, Q. Zhang, J. Dang and C. Xie, *Polym. Adv. Technol.*, 2012, **23**, 1025.
5 J. Gu, J. Dang, Y. Wu, C. Xie and Y. Han, *Polym.–Plast. Technol. Eng.*, 2012, **51**, 1198.
6 J.-W. Gu, G.-C. Zhang, S.-L. Dong, Q.-Y. Zhang and J. Kong, *Surf. Coat. Technol.*, 2007, **201**, 7835.
7 G. C. Stevens and A. H. Mann, *Risks and benefits in the use of flame retardants in consumer products: a report for the*

department of trade and industry, Polymer Research Centre, University of Surrey, Surrey, 1999.
8 H. Ishida and T. Agag, *Handbook of benzoxazine*, Elsevier, Amsterdam, 1st edn, 2011, ch. 7, p. 169.
9 S. Rimdusit and H. Ishida, *Polymer*, 2000, **41**, 7941.
10 S. Tragoonwichian, N. Yanumet and H. Ishida, *J. Appl. Polym. Sci.*, 2007, **106**, 2925.
11 H. R Allcock, *Chemistry and applications of phosphazenes*, Wiley-Interscience, Hoboken, NJ, 2003, p. 19.
12 S. Fei and H. R. Allcock, *J. Power Sources*, 2010, **195**, 2082.
13 H. R. Allcock, *J. Inorg. Organomet. Polym. Mater.*, 2006, **16**, 277.
14 J. Ding and W. Shi, *Polym. Degrad. Stab.*, 2004, **84**, 159.
15 D. Kumar, G. M. Fohlen and J. A. Parker, *Macromolecules*, 1983, **16**, 1250.
16 I. Apivhat and P. Eakachai, *J. Hazard. Mater.*, 2010, **184**, 775.
17 K. Krishnadevi, A. Nirmala Grace, M. Alagar and V. Selvaraj, *High Perform. Polym.*, 2014, **26**, 1.
18 K. Krishnadevi, V. Selvaraj and D. Prasanna, *RSC Adv.*, 2015, **5**, 913.
19 H. Ishida and D. P. Sanders, *Macromolecules*, 2000, **33**, 8149.
20 E. Rafiee, S. Shahebrahimi, M. Feyzi and M. Shaterzadeh, *Int. Nano Lett.*, 2012, **2**, 29.
21 A. Proctor, P. K. Clark and C. A. Pareker, *J. Am. Oil Chem. Soc.*, 1995, **72**, 459.
22 M. Rozainee, S. P. Ngo, S. S. Slem, K. G. Tan, M. Ariffin and Z. N. Zainura, *Bioresour. Technol.*, 2008, **99**, 703.
23 J. Fan, X. Hu and C. Y. Yue, *J. Polym. Sci., Part B: Polym. Phys.*, 2003, **41**, 1123.
24 H. D. Kim and H. Ishida, *J. Phys. Chem. A*, 2002, **106**, 3271.
25 C. F. Wang, Y. C. Su, S. W. Kuo, C. F. Huang, Y. C. Sheen and F. C. Chang, *Angew. Chem., Int. Ed.*, 2006, **45**, 2248.
26 C. S. Liao, C. F. Wang, H. C. Lin, H. Y. Chou and F. C. Chang, *Langmuir*, 2009, **25**, 3359.
27 J. Liu, X. Lu, Z. Xin and C. Zhou, *Langmuir*, 2013, **29**, 411.
28 T. Alizadeh, *Mater. Chem. Phys.*, 2012, **135**, 1012.
29 J. Guo, A. Sun, X. Chen, C. Wang and A. Manivannan, *Electrochim. Acta*, 2011, **56**, 3981.
30 M. Sponton, L. A. Mercado, J. C. Ronda, M. Galia and V. Cadiz, *Polym. Degrad. Stab.*, 2008, **93**, 2025.
31 U. Quittmann, L. Lecamp, W. E. Khatib, B. Youssef and C. Bunel, *Macromol. Chem. Phys.*, 2001, **202**, 628.
32 A. B. Morgan and M. Bundy, *Fire Mater.*, 2007, **31**, 257.
33 C. Siat, M. L. Bras and S. Bourbigot, *Fire Mater.*, 1998, **22**, 119.
34 B. Schartel and T. R. Hull, *Fire Mater.*, 2007, **31**, 327.
35 G. Gallina, E. Bravin, C. Badalucco, G. Audisio, M. Armanini, A. D. Chirico and F. Provasoli, *Fire Mater.*, 1998, **22**, 15.
36 D. Y. Wang, Y. Liu, Y. Z. Wang, C. P. Artiles, T. R. Hull and D. Price, *Polym. Degrad. Stab.*, 2007, **92**, 1592.
37 P. J. Elliot and R. H. A. Whiteley, *Polym. Degrad. Stab.*, 1999, **64**, 577.
38 F. Gao and L. Tong anad Z. Fang, *Polym. Degrad. Stab.*, 2006, **91**, 1295.
39 L. Y. Ling, W. W. Lung, H. K. Ying and H. W. Hsuan, *Thermochim. Acta*, 2004, **412**, 139.
40 G. L. Nelson, *Fire retardancy of polymeric materials*, Marcel Dekker, New York, 2000, p. 1.
41 S. Bourbigot, M. LeBras, R. Delobel and L. Gengembre, *Appl. Surf. Sci.*, 1997, **120**, 15.
42 Y. Y. Yen, H. T. Wang and W. J. Guo, *Polym. Degrad. Stab.*, 2012, **97**, 863.
43 M. Z. Fu and B. J. Qu, *Polym. Degrad. Stab.*, 2004, **85**, 633.